Galaxy clusters as probes for cosmology and dark matter

Elia S. Battistelli[†,***], Carlo Burigana[‡,§,¶,†††], Paolo de Bernardis[†,‡‡‡], Alexander A. Kirillov[‖,§§§], Gastao B. Lima Neto[**,¶¶¶], Silvia Masi[**,‖‖‖], Hans U. Norgaard-Nielsen[††,****], Peter Ostermann[‡‡,††††], Matthieu Roman[§§,‡‡‡‡], Piero Rosati[§§,§§§§] and Mariachiara Rossetti[¶¶,‖‖,¶¶¶¶]

[†]*Dipartimento di Fisica, Sapienza Università di Roma, P.le Aldo Moro 5, I-00185, Rome, Italy*

[‡]*INAF-IASF Bologna, Via Piero Gobetti 101, I-40129 Bologna, Italy*

[§]*Dipartimento di Fisica e Scienze della Terra, Università degli Studi di Ferrara, Via Giuseppe Saragat 1, I-44122 Ferrara, Italy*

[¶]*INFN, Sezione di Bologna, Via Irnerio 46, I-40126, Bologna, Italy*

[‖]*Dubna International University of Nature, Society and Man, Dubna, 141980, Russia*

[**]*Departamento de Astronomia, IAG/USP, São Paulo/SP, 05508-090, Brazil*

[††]*DTU Space, Elektrovej, DK – 2800 Kgs. Lyngby, Denmark*

[‡‡]*independent-research.org, Munich, Germany*

[§§]*Laboratoire de Physique Nucléaire et des Hautes Énergies (LPNHE), Université Pierre et Marie Curie, Paris, France*

[¶¶]*Dipartimento di Fisica, Università degli Studi di Milano, Via Celoria 16, I-20133, Milan, Italy*

[‖‖]*INAF – IASF Milano, via Bassini 15, I-20133 Milano*

[***]*elia.battistelli@roma1.infn.it*
[†††]*burigana@iasfbo.inaf.it*
[‡‡‡]*paolo.debernardis@roma1.infn.it*
[§§§]*ka98@mail.ru*
[¶¶¶]*gastao@astro.iag.usp.br*
[‖‖‖]*silvia.masi@roma1.infn.it*
[****]*hunn@space.dtu.dk*
[††††]*peos@independent-research.org*
[‡‡‡‡]*matthieu.roman@lpnhe.in2p3.fr*
[§§§§]*rosati@fe.infn.it*
[¶¶¶¶]*mariachiara.rossetti@unimi.it*

In recent years, significant progress has been made in building new galaxy clusters samples, at low and high redshifts, from wide-area surveys, particularly exploiting the Sunyaev–Zel'dovich (SZ) effect. A large effort is underway to identify and characterize these new systems with optical/NIR and X-ray facilities, thus opening new avenues to constraint cosmological models using structure growth and geometrical tests. A census of galaxy clusters sets constraints on reionization mechanisms and epochs, which need to be reconciled with recent limits on the reionization optical depth from cosmic microwave background (CMB) experiments. Future advances in SZ effect measurements will include the possibility to (unambiguously) measure directly the kinematic SZ effect, to build an even larger catalogue of galaxy clusters able to study the high redshift universe, and to make (spatially-)resolved galaxy cluster maps with even spectral capability to (spectrally-)resolve the relativistic corrections of the SZ effect.

Keywords: Galaxy clusters; cosmology; background radiations; radio; microwave; observational cosmology; large scale structure of the universe; intracluster matter; dark matter; dark energy.

1. Introduction

Galaxy clusters are among the most studied and interesting objects of our universe. Recent technological improvements have made possible a massive increase of the size of galaxy cluster catalogues and a key role has been played by the full exploitment of the Sunyaev–Zel'dovich (SZ) effect as galaxy clusters searcher. The SZ effect is a powerful tool to study our universe at low and high redshift, to investigate the adiabaticity of the universe expansion, the equation of state of dark energy, the dark matter distribution in the universe, and the astrophysics governing the biggest objects of our Universe. The SZ effect has been historically described by three main contributions: the thermal SZ effect arising from the thermal motion of ionised medium in the intra-cluster medium (ICM), the kinematic SZ effect arising from the peculiar motion of the galaxy clusters, and the relativistic corrections to the SZ effect which originate when one accounts for the relativistic temperatures characterising the ICM.

1.1. *Thermal SZ effect*

The thermal SZ effect[114,115] is a spectral distortion of the cosmic microwave background (CMB) caused by inverse Compton scattering between the CMB photons and a hot electron gas present in the ICM in clusters of galaxies.

A complete derivation of the effect can be found in several reviews.[11,17,101,116] In the nonrelativistic limit, the spectral behavior of the distorted spectrum can be obtained by solving the Kompaneets equation,[64] which yields the occupation number $n(\nu)$ of the radiation energy levels:

$$\frac{\partial n}{\partial t} = \frac{kT_e}{m_e c}\frac{\sigma_T n_e}{x_e^2}\frac{\partial}{\partial x_e}\left[x_e^4\left(\frac{\partial n}{\partial x_e} + n + n^2\right)\right], \tag{1}$$

where n_e is the electron number density, m_e and T_e are the electron mass and gas temperature respectively, σ_T is the Thomson cross-section and $x_e = h\nu/k_B T_e$ (not to be confused with the dimensionless frequency $x = h\nu/k_B T_{\rm CMB}$).

Under the assumption that $T_e \gg T_{\rm CMB}$, the Kompaneets equation admits a simple analytical solution. We define the parameter y as:

$$y = n_e \sigma_T \frac{k_B T_e}{m_e c^2} ct, \tag{2}$$

which represents a dimensionless measurement of the time spent in the electron distribution and can be written in the form:

$$y = \int n_e \sigma_T \frac{k_B T_e}{m_e c^2} dl = \tau \frac{k_B T_e}{m_e c^2}, \tag{3}$$

where the integration is calculated along the line of sight dl, τ is the optical depth and electron temperature T_e has been assumed constant; y is known as the Comptonization paramenter. At low optical depth and low electron temperature, for a Planckian incident radiation spectrum, we get a spectral variation of the occupation number of the form:

$$\Delta n(x) = xy\frac{e^x}{(e^x-1)^2}\left(x\cdot\coth\left(\frac{x}{2}\right)-4\right) \tag{4}$$

and thus the specific intensity change due to thermal SZ effect is:

$$\frac{\Delta I_{\rm TSZ}(x)}{I_0} = x^4 y\frac{e^x}{(e^x-1)^2}\left(x\cdot\coth\left(\frac{x}{2}\right)-4\right) = yg(x), \tag{5}$$

where $I_0 = \frac{2h}{c^2}(\frac{k_B T_{\rm CMB}}{h})^3$.

The spectral behavior of the thermal SZ effect is shown in Fig. 1(a). From the above equations, we can extract the main features of the thermal SZ effect in the nonrelativistic approximation:

- the SZ effect amplitude depends only on y: it linearly depends on the cluster electron temperature and on the optical depth τ (i.e. on the cluster pressure integrated along the line of sight);
- the spectral behavior is described by relatively simple analytical functions (i.e. $g(x)$);
- we have a zero point of the effect for $x = 3.83$ (i.e. $\nu = 217\,\text{GHz}$) with $\Delta I_{\rm TSZ}(x) < 0$ for $x < 3.83$ and $\Delta I_{\rm TSZ}(x) > 0$ for $x > 3.83$;
- the specific intensity is characterized by a minimum value at $x = 2.26$ and a maximum at $x = 6.51$;
- since the SZ effect arises solely from interaction of CMB photons with hot cluster gas and the CMB is a background that exists everywhere, the SZ effect does not suffer spherical dilution or cosmological dimming as an isotropic radiator does; this results in its redshift independence. This is valid also for its spectral behavior under the assumption that the CMB temperature scales with the redshift as

$$T_{\rm CMB}(z) = T_{\rm CMB}(0)(1+z). \tag{6}$$

1.2. *Kinematic SZ effect*

While the thermal SZ effect is due to random thermal motion of the ICM electrons with isotropic distribution, if the cluster has a finite peculiar velocity, one expects an additional kinematic effect due to the electrons motion with respect to the CMB, which causes a Doppler shift of the scattered photons. If one assumes that thermal and the kinematic SZ effect are separable, it is forward to extract the spectral dependence of the kinematic SZ:

$$\frac{\Delta I_{\rm KSZ}(x)}{I_0} = x^4\frac{e^x}{(e^x-1)^2}\frac{v_p}{c}\tau = h(x)\frac{v_p}{c}\tau, \tag{7}$$

where v_p is the peculiar cluster velocity along the line of sight.

The net effect observed on the CMB spectrum is thus a change of the temperature of the Planckian spectrum, found to be higher for negative velocities (i.e. moving toward the observer) and vice versa (see Fig. 1). The kinematic SZ effect is a powerful method to determine peculiar cluster velocities along the line of sight. The spectral coincidence between the maximum intensity of the kinematic effect and the zero point of the thermal effect allows, in principle, to distinguish between them. The spectral behavior of the kinematic SZ effect, is anyway identical to that of the CMB anisotropies: this results in an effective difficulty to disentangle these two effects from their spectral behavior (see Fig. 1(b)).

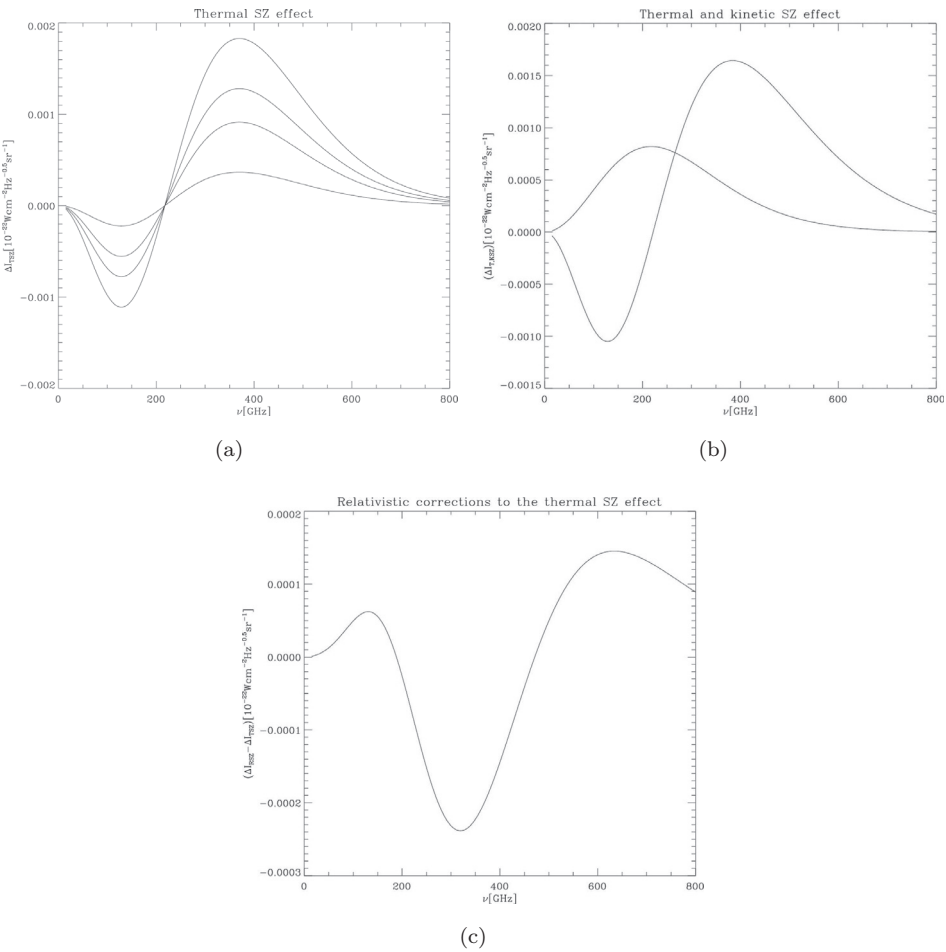

Fig. 1. (a) Thermal SZ effect for $y = 10^{-4}$, 7×10^{-5}, 5×10^{-5}, 2×10^{-5}. (b) Thermal and kinematic SZ effect for $y = 10^{-4}$, $v_p/c = 10^{-3}$ and $T_e = 8.2\,\mathrm{keV}$. The kinematic curve has been multiplied by a factor -10. (c) Relativistic corrections to the SZ effect up to the fifth order in Θ_e for $y = 10^{-4}$, and $T_e = 8.2\,\mathrm{keV}$.

1.3. *Relativistic corrections*

ICM electrons with temperatures from $\simeq 3\,\mathrm{keV}$ are characterized by near relativistic velocities. In order to perform a *more exact* calculation of the SZ effect, one needs to take into account relativistic corrections to it. Taking into account these effects drives to nonnegligible corrections of the order of a few percent of the thermal SZ effect itself.

Different methods have been proposed in order to deal with this problem: a numerical approach consists in performing Monte Carlo simulations of interactions between electrons and photons in a fully relativistic regime. The analytical approach allows to explicit the relativistic correction in terms of powers of the electron cluster temperature.

The inadequacy of the Kompaneets equation had already been considered early in 1979 by Wright[122] and in 1981 by Fabbri[36] who have extended the formalism to the case of little number of scatterings. An explicit treatment for typical cluster temperatures has been presented by Rephaeli in 1995,[102] who has stressed, in agreement with Itoh *et al.*[50] the shift of the zero point frequency x_0 of the thermal SZ effect: x_0 is pushed to higher values with increasing electron temperature $\Theta_e = \frac{k_B T_e}{m_e c^2}$. Challinor *et al.*[19] focused of the corrections in the Rayleigh–Jeans part of the spectrum while a second-order approximation which takes into account additional corrections related with the peculiar cluster velocity has been found by Sazonov and Sunyaev.[108] An analytical fitting formula for the relativistic corrected thermal SZ effect, $\frac{\Delta I_{\mathrm{T}_R\mathrm{SZ}}(x)}{I_0}$ up to the fifth-order in Θ_e has been reported by Itoh *et al.*[50]:

$$\begin{aligned}\frac{\Delta I_{\mathrm{T}_R\mathrm{SZ}}(x)}{I_0} &= yx^4\frac{e^x}{(e^x-1)^2}(Y_0+\Theta_e Y_1+\Theta_e^2 Y_2+\Theta_e^3 Y_3+\Theta_e^4 Y_4)\\ &= y g_{\mathrm{rel}}(x,T_e),\end{aligned} \tag{8}$$

where Y_n are a set of functions depending on the dimensionless frequency only. The spectral behavior of the relativistic corrections to the thermal SZ effect is shown in Fig. 1(c), once subtracted by the uncorrected thermal SZ spectrum.

Nozawa *et al.*[81] have added to the above expression the terms originated by the effect of the peculiar cluster velocity, while Itoh *et al.*[51] have extended the relativistic correction up to the seventh-order in power of Θ_e and Shimon and Rephaeli[110] have found an accurate expression of the cross over frequency up to the fourth-order in Θ_e considering also the dependence on τ.

In the relativistic corrected treatment the spectral behavior of the thermal SZ effect is thus dependent on T_e and the one of the kinematic SZ effect depends on both T_e and v_p. Multifrequency observations of the SZ effect are necessary to disentangle the different effects. In principle, one could use the kinematic SZ and the relativistic corrections of the SZ effect to infer the properties of the galaxy clusters.

2. The SZ Effect as Cosmological Probe

2.1. *Absolute CMB temperature at galaxy cluster redshift: The Melchiorri–Rephaeli method*

The possibility to use multifrequency observations of the SZ effect to constrain the absolute temperature of the CMB at the redshift of the observed galaxy cluster was already suggested long ago by Fabbri *et al.*[35] and by Rephaeli[100] who have proposed the method independently. Francesco Melchiorri and Yoel Rephaeli have first applied and led these analyses since then,[74,103] demonstrating the method capability when the first multifrequency millimetric SZ measurements have been available. We here propose to name this method after them: the *Melchiorri–Rephaeli* method (M–R method). The proposed analysis is based on the steep frequency dependence of the change in the CMB spectral intensity, $\Delta I_{\rm SZ}$, due to the effect, and the weak dependence of ratios $\Delta I_{\rm SZ}(\nu_i)/\Delta I_{\rm SZ}(\nu_j)$ of intensity changes measured at two frequencies (ν_i, ν_j) on properties of the cluster. Because of this, and the fact that, in the Standard Model (SM) the effect is redshift-independent, SZ measurements have the potential of yielding much more precise values of $T_{\rm CMB}(z)$ that can be obtained from atomic and molecular lines detection. With the improved capability of reasonably precise spectral measurements of the SZ effect, the M–R method can now be used to measure $T_{\rm CMB}(z)$ in a wide range of redshifts.

The M–R method has been applied for the first time to SZ measurements performed by MITO experiment on Abell 1656[30] and by SuZIE experiment on Abell 2163[48] clusters of galaxies[7] and several other SZ measurements have been used since then.[29,49,65,69,70,78,88,97,106] This measurement can effectively yield very precise measurements of $T_{\rm CMB}(z)$ which will tightly constrain alternative models for the functional scaling of the CMB temperature with redshift, and thereby provide a strong test of nonstandard cosmological models. Lima *et al.*[67] assume an "adiabatic photon creation" which takes place for instance because of a continuous decaying vacuum energy density or some alternative mechanisms of quantum gravitational origin. A functional form which seems also to be of some theoretical interest is described by LoSecco *et al.*[68]:

$$T_{\rm CMB}(z) = T_{\rm CMB}(0)(1+z)^{1-\beta}. \tag{9}$$

Obviously, in the SM $\beta = 0$. More generally, deviations from isotropy and homogeneity or models in which ratios of some of the fundamental constants vary over cosmological time are also of considerable interest. A precise determination of $T_{\rm CMB}(z)$ would allow to put constraints on the variation of the fundamental constants over cosmological time giving thus important information about the previously cited alternative theories or other exotic cosmologies. So far the best limits for arising from the M–R method are obtained by the *Planck*[a] data to the percentage

[a] *Planck* is a project of the European Space Agency — ESA — with instruments provided by two scientific Consortia funded by ESA member states (in particular, the lead countries: France and

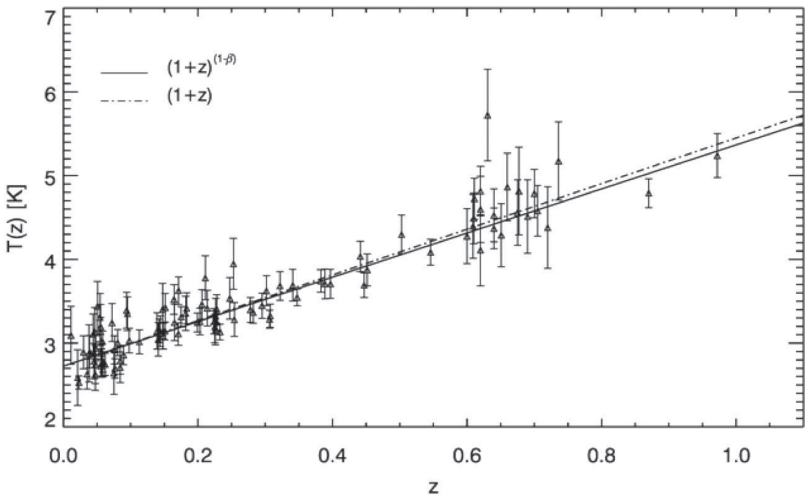

Fig. 2. Measurements of the CMB temperature as a function of redshift for 104 *Planck* selected clusters. The solid line is the best fit to the scaling $T_{\rm CMB}(z) = T_{\rm CMB}(0)(1+z)^{1-\beta}$. The dot-dashed line is the standard scaling, with $\beta = 0$. Picture taken by Luzzi *et al.*[70] see there for details (courtesy G. Luzzi).

level in β[4,70] (see Fig. 2). It is worth noting that further limits on these alternative cosmologies will be achieved through CMB spectral distortions measurements[20] but it is also clear that a new phenomena/physics has to be hypothesized in case $\beta \neq 0$ is found.

2.2. *SZ as baryonic dark matter searcher*

The SZ effect also represents a unique probe to study the baryon distribution in our universe enabling us to solve, at least in part, the apparent discrepancy between the observed baryon distribution in the local universe (by HI absorption, gas and stars in galaxy clusters and X-ray emission, $\Omega_b \simeq 0.021$)[39] as compared to the one predicted by nucleosynthesis, by Ly-alpha forest and by CMB power spectrum observations ($\Omega_b \simeq 0.049$).[97] A diffuse baryonic dark matter is in fact predicted by simulations[18,25,111] in the form of warm-hot intergalactic medium (WHIM). Detections have been performed in the ultraviolet and soft X-ray bands[15,80,119] but most of them are ambiguous or controversial and they lack of a confirmation by later studies.[123] The presence of WHIM could be detectable via SZ effect, especially in super-clusters of galaxies (SCG) where the intra-supercluster medium (ISCM) may be sufficiently dense, hot or characterized by large line of sights, to be seen through the SZ effect even if no clusters of galaxies are present in that region. Search for this kind of signature have been performed with different approaches, either via direct measurements[9,40,91] or cross correlating CMB maps with matter tracing

Italy) with contributions from NASA (USA), and telescope reflectors provided in a collaboration between ESA and a scientific Consortium led and funded by Denmark.

templates.[113] The first clear detection of filamentary structures was performed by the *Planck* Collaboration in the intermediate release[91] for the merging cluster pair A399–A401, and three more in 2015 results.[98] Van Waerbeke *et al.*[120] reported a positive correlation between maps reconstructed from the Canadian France Hawaii Telescope Lensing Survey and a thermal SZ map constructed from *Planck* data. They interpreted this correlation as arising from WHIM at $z \simeq 0.4$ with temperature in the range 10^5–10^6 K.

This research field has enormously benefited by the high sensitivity, wide spectral coverture, and improved angular resolution obtained with the *Planck* satellite. Finer angular resolution, improved sensitivity, and deeper control of foreground removal, together with improved cross-correlation techniques, will allow to shed a definitive light on this still open problem.

2.2.1. *The collapsing supercluster* SC0028 − 0005 *at redshift* 0.22

Besides being possible locations to search for baryonic dark matter, superclusters of galaxies are of tremendous astrophysical interest to understand the ΛCDM standard structures formation scenario and multi-frequencies studies have to be performed for a deep understanding of the underlying physics. Superclusters of galaxies are in fact collapsing objects, barely out of the linear evolution phase of the primordial density fluctuations. The low density contrast between supercluster and the field, just above unity, makes their detection burdensome. Moreover, given their large size their dynamical analysis is difficult and only a few superclusters have been thoroughly studied up to now (see e.g. Refs. 33, 6 and 79).

The supercluster SC0028-0005[83] at redshift 0.22 was used to investigate the structure and dynamics of a super-cluster, which was first detected by Basilakos[5], who used a percolation algorithm applied to the cluster catalogue of Goto.[43] Using the Sloan Digital Sky Survey Data Release 10, all member galaxies within 1.2 degrees from the supercluster center were selected.

The clusters and groups comprising the supercluster were identified by determining the highest density peaks in the projected 2D density distribution, with the constraint that these structures should be dominated by a red population of galaxies. Six clusters (or groups) members were then used as probes of the cluster dynamics.

A multi-band observation done with MegaCam/CFHT was also used to derive the mass distribution inside the supercluster based on weak-lensing effect. The mean seeing was 0.5″ and the data processing was done by the Terapix team.

The 3D spatial distribution was determined by measuring the fundamental plane of elliptical galaxies. Once the distance was known, the peculiar line-of-sight velocity could be retrieved. The supercluster mass distribution was estimated by applying the spherical collapse model within the context of a ΛCDM cosmology. The equation of motion of a spherical shell together with the background Friedman–Lemaître equation were solved simultaneously.

The dynamical analysis suggests that SC0028 is indeed a collapsing supercluster, supporting the ΛCDM standard formation scenario of these structures. The mass within $r = 10\,\mathrm{Mpc}$ was estimated to lie between 4 and $16 \times 10^{15} M_{\odot}$. The farthest detected members of the supercluster imply that within ∼60 Mpc the density contrast is $\delta \sim 3$ with respect to the critical density at the supercluster redshift, so that the total mass is ~ 4.6–$16 \times 10^{17} M_{\odot}$, most of which is in the form of galaxy group sized or smaller substructures. More details can be found in Ref. 82.

2.3. *SZ versus X-ray emission*

As it is well known, thermal SZ and X-ray emissions sample the same ICM with different properties. This is due to the fact that the SZ effect is proportional to the pressure integrated along the line of sight, $\Delta I_{\mathrm{SZ}} \propto \int n_e T_e dl$ while the X-ray emission depends on the cluster characteristics in different way: $S_x \propto \int n_e^2 \Lambda_X dl$, where Λ_X is the X-ray cooling function, weakly depending on T_e. Joint analysis of the SZ and X-ray data allows to study the pressure profiles of galaxy clusters and brake degeneracy between the ICM gas density and the cluster angular diameter distance.

This analysis has been historically used for the determination of the Hubble constant H_0.[8,17] This has the great advantage to be independent on extragalactic standard candles; on the other hand, the method is found to be affected by calibration uncertainties[99] and by the accurate modeling of the cluster density and temperature profile.[13] Early measurements assumed the gas to be isothermal and tended to underestimate H_0. So does a departure from the sphericity of the galaxy cluster if the cluster is elongated along the line of sight (and vice versa). More recent studies account for radial temperature profile of T_e but direct temperature measurements are available only up to about one third of the viral radius from spatially resolved X-ray measurements and rely on simulations for a careful determination of the temperature profile.[61] The fact that many galaxy clusters are often aspherical, far from being relaxed and well approximated by a standard profile increases the scatter in these measurements. In addition, offsets between the X-ray emission and the SZ peaks in merging clusters have cosmological implications.[124] Selection bias may also apply as elongated-along-the-line-of-sight clusters are statistically more prone to be observed. Clumpiness in the gas density tend to overestimate H_0 while inhomogeneities of the temperature underestimates it. All this, not to account for point source contamination in the SZ measurements.

Similar analysis can be performed for the determination of the gas mass fraction of galaxy clusters.[61] Reversing the argument, one can try to infer galaxy cluster properties and any departure from the distance duality relation using the same SZ and X-ray observations assuming cosmological parameters including H_0 from other measurements.

3. SZ as Clusters Finder

Thanks to its redshift independence, the SZ effect can actually be used to discover galaxy clusters in blind large-area microwave maps enabling, through optical follow-up observations, an effective count of galaxy clusters as a function of the redshift. Galaxy cluster counts are a standard cosmological tool that has found powerful applications. The spectral distortion imprinted on CMB by the SZ effect can be easily recognized with a multi-frequency high-sensitivity instrument like *Planck* or with improved angular resolution surveys as in the case of the Atacama Cosmology Telescope (ACT) or the South Pole Telescope (SPT). Recent studies have demonstrated the SZ effect to be a very efficient method to detect clusters,[12,45] and to provide a complementary view to X-rays to study ICM properties, especially in the faint outer regions.[34,89,90] The sample of galaxy clusters observed through the SZ effect has been enlarged by more than an order of magnitude in the last decade.[12,45,96]

The ability to find a galaxy cluster in a microwave/millimetric map is mainly related to the cluster flux and mass. A typical galaxy cluster at redshift $\simeq 1$ has a size in the sky of the order of 2 arcmin and an adequate angular resolution has to be achieved in order to efficiently detect distant clusters. The ACT[46] and the SPT[112] have been designed to achieve such an angular resolution. ACT and SPT have been able to find clusters down to $M_{500} \simeq 1.5 \cdot 10^{14}$ solar masses up to $z \simeq 1.5$ (where M_{500} is the cluster mass enclosed in R_{500} which corresponds to a radius within which the average matter density is 500 times the critical matter density of the universe). Despite *Planck* experiment is characterized by a more moderate angular resolution, it has performed a full sky survey with much wider frequency coverage. This makes *Planck* more stable for observing nearby clusters[b] with respect to ACT and SPT. The SPT has been the first experiment to blindly detect a galaxy cluster[112] and, since then, 516 optically confirmed clusters have been found by the SPT,[12] 91 by the ACT[45] and 1094 by *Planck*.[96] See Fig. 3 for a resume of the current SZ discovered clusters with their mass as a function of the redshift.

The abundance of clusters and its evolution are sensitive to the cosmic matter density, $\Omega_{\rm m}$, and the present amplitude of density fluctuations, characterized by σ_8, the RMS linear overdensity in spheres of radius $8h^{-1}$ Mpc, as well as the nature of dark energy. CMB anisotropies reflect the density perturbation power spectrum at the time of recombination. A comparison of the two can be used to test the evolution of density perturbations from recombination until today, enabling us to look for possible extensions to the base ΛCDM model.

One of the importance of studying the SZ clusters number counts, is that it is mainly independent from other cosmological probes like baryonic acoustic oscillations (BAO), Super Novae Ia measurements and even primary CMB anisotropies

[b]Part of this paper is based largely on the products available at the ESA *Planck* Legacy Archive and publicly available publications by ESA and the *Planck* Collaboration, for what concerns the related aspects. Any material presented here that is not already described in *Planck* Collaboration papers represents the views of the authors and not necessarily those of the *Planck* Collaboration.

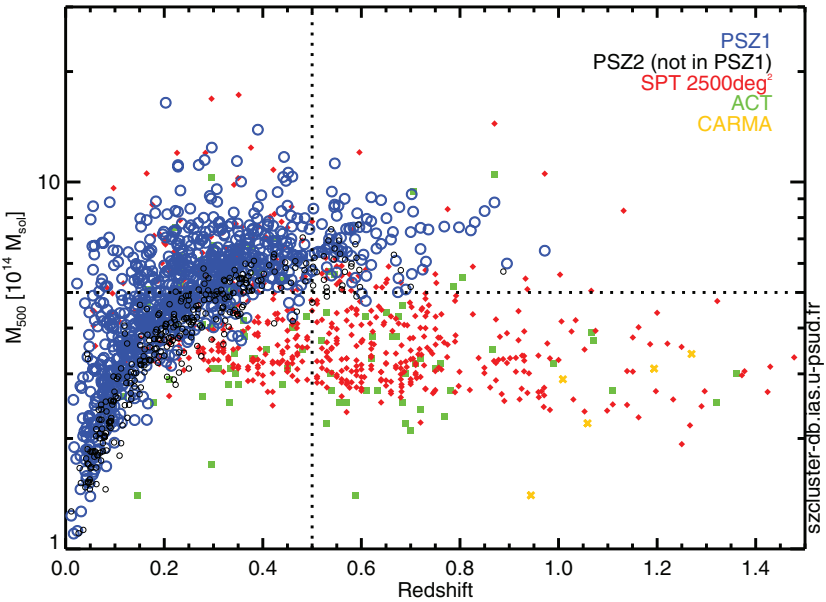

Fig. 3. Clusters detected by ACT, SPT and *Planck* (as well as Carma[14]) as a function of redshift. This compilation was downloaded from http://szcluster-db.ias.u-psud.fr.

measurements. A fundamental point is however related to the ability to determine the galaxy clusters mass to which any use of the number counts as cosmological probe is sensitive to. This is particularly critical for high redshift clusters for which spatially resolved X-ray imaging and gravitational lensing estimates are more and more difficult. In this sense, we can rely on the scaling *Y-M* relations between observed SZ distortion parameter and cluster mass. Despite being still uncertain, these scaling relations are already being used and will make the SZ even a more powerful tool in future surveys.

Comparison, in the 2013 *Planck* release, between estimates of σ_8 and $\Omega_{\rm m}$ from clusters number counts and from primary CMB anisotropies found inconsistent results. Despite being sensibly relaxed in the 2015 *Planck* release (see Sec. 3.2), the origin of this tension is not completely sorted out. Besides the possibility of an incomplete instrumental calibration, this tension could be reconciled assuming underestimate of the true clusters masses or missing an important fraction of clusters, which would have driven to an underestimation of σ_8 in the cluster counts analysis, or assuming a variation of initial perturbation spectrum and/or suppression of density fluctuations at small scales (like those possibly produced by massive neutrinos), which would have driven to an overestimation of σ_8 in the primary CMB analysis.

It is worth noting though that, as shown by Hasselfield *et al.*,[45] different *Y-M* scaling relations have a large impact on the Ω_m, σ_8 determination. Reversing the argument one could use the SZ counts with CMB measurements to infer the *Y-M* scaling relation normalization.

3.1. *The second Planck catalogue of SZ sources*

In this section, we present the Second *Planck* Catalogue of Sunyaev-Zel'dovich sources (PSZ2 hereafter), which is part of the 2015 *Planck* full-mission data release.[96] The PSZ2 is the third catalogue of galaxy clusters detected by *Planck*, after the ESZ,[88] containing 189 detections from the first months of data, and the PSZ1,[93] containing 1227 sources detected by *Planck* in its nominal mission (15.5 months). The PSZ2 contains 1653 clusters candidates detected from the full mission data (29 months with both LFI and HFI instruments) with a signal-to-noise ratio (SNR) larger than 4.5 on 83.6% of the sky (excluding the Galactic plane and known point sources). The catalogue is publicly available in the *Planck* Legacy Archive (PLA, http://pla.esac.esa.int/pla/), along with the survey completeness function (we refer to the PSZ2[96] and PSZ1[93] papers for details on data analysis and for a description of the products in the archive).

The SZ observable is the integrated Comptonization parameter $Y_{\rm SZ}$, which is measured in the *Planck* catalogues on a scale of $5R_{500}$. Since the SZ parameter is strongly degenerate with the cluster size, the *Planck* Collaboration provided for each detection the two-dimensional posterior distribution for Y_{5R500} and the scale radius θ_s. The value Y_{5R500} provided in the catalogues is the expected value of the marginal distribution and is shown to be unbiased at a few percent level. This measurement could be possibly rescaled to the more physically interesting Comptonization parameter on the R_{500} scale by assuming a pressure profile. However, a posterior analysis has shown that this procedure returns strongly biased results. Therefore, to estimate Y_{500} (and thus M_{500}) from *Planck* data, it is necessary to break the size-flux degeneracy by using prior information, relating Y_{500} and θ_{500} using the definition of M_{500} and the $Y_{500} - M_{500}$ scaling relation.

A necessary element to characterize a survey is the selection function, both in terms of completeness (i.e. the probability that an object with a given observable is detected in the survey) and of statistical reliability, or purity (i.e. the probability that a detection with a given SNR is a real cluster). The completeness is a function of both the cluster size θ_{500} and the SZ flux Y_{500} and is available in the PLA for different SNR thresholds. It was estimated for the PSZ2 with two independent methods that provided consistent results: Monte Carlo injection in simulated maps and a semi-analytical treatment (assuming Gaussian noise). Monte Carlo simulations were also used to assess the survey reliability: its lower limit is 83% for a SNR threshold of 4.5, but it rapidly increases with SNR. The reliability is higher if we apply a more selective mask excluding a larger region around the Galactic plane and if we apply a higher SNR threshold, as in the subsample used for measuring cosmological parameters with galaxy clusters.[95]

Searching for counterparts is an important part of the catalogue construction, because it allows to validate the PSZ2 detections and to associate redshifts (necessary for breaking the size-flux degeneracy and thus measure the mass and the integrated signal) to the confirmed detections. This procedure is based on the well-

validated PSZ1 catalogue and complemented with multi-wavelengths ancillary data sets (microwave, IR, optical and X-ray catalogues) and each possible counterpart association has been confirmed by analysis of scaling relations. 1094 detections in the PSZ2 were associated to a known counterpart with redshift: the PSZ2 is thus the first SZ catalogue with more than one thousand confirmed objects and the largest SZ-selected sample of galaxy clusters.

In Fig. 3, in addition to the ACT, SPT and Carma clusters, the distribution of the *Planck*-detected clusters with counterpart in the mass-redshift plane, along with the expected completeness curves, is shown. The new PSZ2 detections are mostly low mass objects close to the detection limit of the survey in all redshift ranges. We should stress that the distribution in Fig. 3 is not fully representative of the experiment selection, since only points with an associated redshift could be plotted. For instance, at high redshifts ($z > 0.6$) most clusters are PSZ1 detections which were validated through dedicated follow-up. A similar follow-up campaign on the almost 600 cluster candidates in PSZ2 would populate further the $M - z$ plane and allow to characterize many new interesting objects.

3.2. *Science with the Planck SZ* 2015 *cluster sample*

The first *Planck* 2013 cluster analysis found fewer clusters than predicted by *Planck*'s base ΛCDM model, expressed as tension between the cluster constraints on $(\Omega_{\rm m}, \sigma_8)$ and those from the primary CMB anisotropies.[92] This could reflect the need for an extension to the base ΛCDM model, or indicate that clusters are more massive than determined by the SZ signal-mass scaling relation adopted in 2013.

The cluster mass scale is the largest source of uncertainty in interpretation of the cluster counts. We based our first analysis on X-ray mass proxies that rely on the assumption of hydrostatic equilibrium. We quantified our ignorance of the true mass scale of clusters with a mass bias parameter that was varied over the range [0–30]%, with a baseline value of 20%, as suggested by numerical simulations (see the Appendix of Ref. 92).

New, more precise lensing mass measurements for *Planck* clusters have appeared since then. In addition, we apply a novel method to measure cluster masses through lensing of the CMB anisotropies. We incorporate these new results as prior constraints on the mass bias in the present analysis: $1-b = 0.688 \pm 0.072$ from Weighing the Giants (WtG[121]), $1-b = 0.780 \pm 0.092$ from the Canadian cluster comparison project (CCCP[47]) and $1/(1-b) = 0.99 \pm 0.19$ from *Planck* CMB lensing.[75] Two other improvements over 2013 are the use of a larger cluster catalogue and the analysis of the counts in signal-to-noise as well as redshift.[95]

We define a cosmological sample from the general PSZ2 catalogue,[96] consisting of detections by the MMF3 matched filter. It is defined by a signal-to-noise (denoted q) cut of $q > 6$. We then apply a mask to remove regions of high dust emission and point sources, leaving 65% of the sky unmasked. The MMF3 sample contains 439

detections and spans masses in the range $[2\text{–}10] \times 10^{14}\, M_\odot$ and redshifts from $z = 0$ to 1.

The distribution of clusters in redshift and signal-to-noise can be written as

$$\frac{dN}{dzdq} = \int d\Omega_{\rm mask} \int dM_{500}\, \frac{dN}{dzdM_{500}d\Omega}\, P[q|\bar{q}_{\rm m}(M_{500}, z, l, b)], \tag{10}$$

with $dN/dzdM_{500}d\Omega$, the dark matter halo mass function times the volume element. We adopt the mass function from Ref. 118. The quantity $P[q|\bar{q}_{\rm m}(M_{500}, z, l, b)]$ is the distribution of q given the mean signal-to-noise value predicted by the model for a cluster of mass M_{500} and redshift z located at Galactic coordinates (l, b). This latter quantity is defined as the ratio of the mean SZ signal expected of a cluster, $\bar{Y}_{500}(M_{500}, z)$, and the detection filter noise, $\sigma_{\rm f}[\bar{\theta}_{500}(M_{500}, z), l, b]$. The redshift distribution of clusters detected at $q > q_{\rm cut}$ is the integral of Eq. (10) over signal-to-noise given $\chi(Y_{500}, \theta_{500}, l, b)$, the survey selection function at $q > q_{\rm cut}$.

We divide the catalogue into bins of size $\Delta z = 0.1$ (10 bins) and $\Delta \log q = 0.25$ (5 bins), each with an observed number $N(z_i, q_j) = N_{ij}$ of clusters. Modeling the observed counts as independent Poisson random variables, our log-likelihood is

$$\ln L = \sum_{i,j}^{N_z N_q} [N_{ij} \ln \bar{N}_{ij} - \bar{N}_{ij} - \ln[N_{ij}!]], \tag{11}$$

where N_z and N_q are the total number of redshift and signal-to-noise bins, respectively. The mean number of objects in each bin is predicted by theory according to Eq. (10) which depends on the cosmological (and cluster modeling) parameters. In practice, we use a Monte Carlo Markov Chain (MCMC) to map the likelihood surface around the maximum and establish confidence limits.

We combine all SZ cluster counts results with Big Bang Nucleosynthesis (BBN) constraints and BAO. We vary all six parameters of the (flat) base ΛCDM model, except when considering model extensions for which we include the relevant parameters. Counts are consistent with those from 2013 and yield comparable constraints.

The central value of the WtG mass prior lies at the extreme end of the range used in 2013; with its uncertainty range extending even lower, the tension with primary CMB is greatly reduced, as pointed out by Ref. 121. With similar uncertainty but a central value shifted to $1-b = 0.78$, the CCCP mass prior results in greater tension with the primary CMB. The lensing mass prior, finally, implies little bias and hence much greater tension.

We obtain the posterior on $(1 - b)$ from a joint analysis of the MMF3 cluster counts and the CMB with the mass bias as a free parameter. The best-fit value in this case is $(1-b) = 0.58 \pm 0.04$, more than 1σ below the central WtG value. Perfect agreement with the primary CMB would imply that clusters are even more massive than the WtG calibration. This case most clearly quantifies the tension between the *Planck* cluster counts and primary CMB. Allowing $\tau_{\rm reion}$ to adjust offers only minor improvement in the tension.

The SZ counts (2D likelihood with CCCP prior) only marginally break the dark energy degeneracy when combined with the CMB, but when combined with BAO they do yield interesting constraints that are consistent with the independent constraints from the primary CMB combined with supernovae.

Increasing neutrino mass goes in the direction of reconciling tension between the cluster and primary CMB constraints, but would necessarily increase tension with some direct measurements of H_0 and with BAO. The lensing power spectrum, in favoring slightly lower σ_8, reinforces the cluster trend so that a peak appears in the posterior for $\sum m_\nu$; it is not enough, however, to bring the posterior on the mass bias in line with the prior. This indicates that the tension between the cluster and primary CMB constraints is not fully resolved.

With a number of improvements and new information relative to our first study (more data, 2D likelihood), we confirm the 2013 results. We extract cosmological constraints using three different cluster mass scales and find that the value needed for the mass bias to bring cluster counts and CMB primary anisotropies in full agreement is larger than the used priors, suggesting a tension at the astrophysical level or indicating a need for extension of the baseline cosmological model. A precision of 1% on the cluster mass, targeted by future large lensing surveys such as *Euclid* and LSST, would significantly clarify the extent of any tension.

3.3. *Planck* 2015 *vs SZ cluster counts*: *An alternative cosmological model to explain the mismatch*

In view of the *Planck* 2015 model prediction mismatch of SZ cluster counts it seems intriguing to test also a recently found mathematical chance of a universal microwave background composed of redshifted radiation emitted from a homogeneously distributed part of 'dark' matter (hDM) (for details, see Ref. 85). Within a stationary Universe the additional part might exist instead of the 'dark energy' assumed today. According to that solution the SZ effect would stay present, though increasingly weakened with redshift. A corresponding gradual shift of the SZ spectral profile to lower frequencies seems ruled out at first sight. With respect to the subtraction of unavoidable noise and various 'foregrounds', however, a definite clarification seems more difficult than expected. In particular, the existence of the CIB as well as the nature of inhomogeneities of the whole microwave background have to be taken into a new consideration to clarify this question seriously.

Inhomogeneities of the alternative CMB, for example, might also cause some frequency shift, thereby compensating a small frequency shift in parts. Measurements in the bands $\geq 218\,\mathrm{GHz}$ seem particularly problematic. The results have been mostly relying on smaller frequencies before, which in view of unknown individual masses seem to make no clear differences between both alternatives of the thermal SZ in cluster count ranges $z < 1$.

Actually it cannot be safely excluded, that the *Planck* 2015 model prediction mismatch might partially arise from a correspondingly reduced signal-to-noise ratio.

Indeed, *Planck*'s major objectives encompassing tests for theories of inflation and providing a direct probe into the Concordance Model's initial inhomogeneities are mainly focused on the ΛCDM cosmology.

According to a new Stationary Universe Model (SUM)[84,86] straightforwardly in accordance with the SNe Ia data on universal scales ($z > 0.1$)[85] the alternative CMB solution requires an attenuation $1/(1+z)^2$ of intensity in the mm range (due to $k = 2/RH$ in addition to the usual photon energy loss by redshift). It is obvious that a gradual reduction of the SZ intensity (up to e.g. 1/4 the value expected for clusters at $z = 1$) would lead to a steeper '$q = 6$' slope down from the third redshift bin in Figs. 4 or 6 of Ref. 96, while other 'free' parameters may be adjustable to match the absolute values of the first and second redshift bin, too.

Though it seems sure that an explanation can be found within the highly adaptable ΛCDM framework, there may be a scientific obligation to falsify the tentative SUM approach in particular by evaluation of the *Planck* 2015 model mismatch of predicted SZ cluster counts, in this case without any ΛCDM priors temporarily.

4. Intra Cluster Medium Physics

The SZ effect is clearly a powerful tool also to study the astrophysics of galaxy clusters themselves. This represents a complementary and alternative method with respect to the classic use of X-ray observations, especially for distant clusters and in the low density cases. Spatially resolved SZ measurements of the thermal and dynamical state of the ICM in groups and clusters can provide, alone, radial profiles of the electron pressure up to larger distances with respect to X-ray observations. Once combined with X-ray observations, high angular resolution SZ measurements promise to recover the n_e and T_e profiles thus providing a unique tool to test models and simulations. This is of fundamental importance for the comprehension of the structure formation and to study turbulent and distant-from-equilibrium scenarios.

The physical state of the ICM depends on several studied and simulated effects as warming up processes, radiative cooling, star formation, cosmic rays, magnetic fields and thermal feedback. The presence of cooling cores and the effect of merging processes still need to be fully understood. Nonthermal electrons also produces CMB photons scattering and cross correlation between synchrotron and SZ emission maps would be fundamental to understand the underlying energy distribution of nonthermal electrons and to verify predictions.[22,38] Nonthermal pressure effects seem to be of fundamental importance at large distances from the cluster center thus making the SZ a possible unique tool for the understanding the galaxy cluster physics. Multi mergers complexes are excellent laboratories for high angular resolution SZ observations in order to reveal temperature and pressure gradients as well as dynamical state of the clusters sub-structures. Merging activity has been detected toward a few clusters including *el Gordo* (i.e. ACT-CL J0102-4915)[76] deserving further studies. High angular resolution studies provide a key consistency check for the mass estimations assuming hydrostatic equilibrium. The presence

of radio sources within a cluster of galaxies is clearly a source of disturbance for SZ measurements. The possibility to remove their effect depends on the angular resolution of SZ observations. Radio emission studies of some clusters reveal the presence of magnetic fields and cosmic rays which are of fundamental importance to understand the energy budget of such galaxy clusters. About 10% of the galaxy cluster are so called "radio loud". They show diffuse synchrotron emission arising from halos, relics and mini-halos.

Early high resolution (i.e. beam$\simeq$ 13") SZ studies made with the Nobeyama telescope have for instance allowed us to understand that previously hypothesized relaxed clusters are, indeed, into a merging activity.[63] The same RX J1347.5-1145 cluster was also observed by MUSTANG from GBT (beam$\simeq$9"),[71] CARMA (synthesized beam$\simeq$11" $\times$ 17")[87] and NIKA from IRAM 30-m(beam$\simeq$18.5").[1] Ferrari *et al.*[37] found a correspondence between the mini-halos emission and the high angular resolution SZ emission detected with the MUSTANG experiment mounted on the GBT[31] which can be explained as gas oscillations within the gravitational potential (i.e. sloshing[73]). BOLOCAM[41] and MUSTANG observations have studied the galaxy cluster pressure profiles in Abell 1835 and MACS-0647[104] while Sayers *et al.*[107] performed an analysis over 45 massive clusters cross correlating SZ and X-ray measurements and studying in details relaxed, disturbed and cool-core clusters. Such observations are in fact enabling, among the rest, to begin understanding the galaxy cluster pressure profiles, the mass-Comptonization scale relations, and to start investigating the thermal state of the ICM in the outskirts of galaxy clusters. Nevertheless, the picture is not complete. Both efforts, NIKA on IRAM and MUSTANG on the GBT are being upgraded with NIKA2[16] and MUSTANG2[32] instruments allowing to enlarge the focal planes and the fields of view (f.o.v.) reducing thus the need to rely on larger-f.o.v./lower-angular-resolution experiments in order to retrieve the large angular scales in their maps. Of clear interest is also the effort spent by the AMI and CARMA Collaborations to study the radio/microwave emission of galaxy clusters with resolutions that can get to $\simeq 0.3$ arcmin.[2] A key opportunity is also represented by the newly built 64 m Sardinia radio telescope[24] which, thanks to its primary reflector active surface, provides a good efficiency up to 100 GHz and is now opening to the scientific community.[c]

5. SZ as Speedometer

As mentioned in Sec. 1.2, the kinematic SZ effect is in principle a powerful method to retrieve the peculiar velocity, along the line of sight, of the electrons of the ICM. This is important both to study the dynamics within galaxy clusters with high angular resolution observations, for instance, in the violent merger cases, and to measure the overall gas velocity in a highly complementary way with respect to future high-dispersion X-ray spectroscopic observations such as those planned by the *Athena+* mission.[79]

[c] http://www.srt.inaf.it/media/uploads/astronomers/avpaperi.v4b.pdf.

Millimetric/multifrequency observations are needed to disentangle the thermal SZ and the kinematic SZ effects for a direct detection of the kinematic effect itself. First pioneeristic millimetric observations of the SZ effect have been made by MITO[30] and SuZIE[48] experiments. SuZIE II experiment gave the first attempt to determine peculiar velocities on six galaxy clusters providing, upper limits.[10]

The first evidence of the motions of galaxy clusters through their kinematic SZ signal has been provided using the 148 GHz maps of the ACT experiment, cross-correlating it with the baryon oscillation spectroscopic survey (BOSS) in the Sloan Digital Sky Survey III.[44] This is a statistical detection which relies on a mean pairwise momentum estimation on the microwave maps, using the BOSS catalog as galaxy clusters proxies. On the other hand, direct incredibly high line-of-sight velocity of $v_p = -3450 \pm 900\,\mathrm{km/s}$ was reported by the BOLOCAM Collaboration using data at 140 GHz and 270 GHz.[107]

A full investigation of the galaxy clusters motions is clearly still at the primordial stage. Difficulty in disentangling the thermal and kinematic SZ effect, and the latter from other sources of disturb is clearly hampering the full exploitation of this methodology. In addition, the mixing of different effects, including the relativistic corrections, makes it even harder.

5.1. *On scattering of CMB radiation on wormholes: Kinematic SZ-effect*

Wormholes as candidate for dark matter particles have also been studied.[53,54,57] The final choice requires the direct observation of effects related to wormholes. We suggest to use the kinematic SZ effect[116,117] which is known to have the universal nature and is long used to study peculiar motions of clusters and groups, e.g.[44,52,105] (for details see Ref. 60). In the present section, we consider the scattering of CMB radiation on wormholes and show that wormholes also contribute to kinematic SZ effect and can be observed in voids. Stable cosmological wormholes have throat sections in the form of tori.[59] Upon averaging over orientations such tori can be considered as spheres, and therefore, we use for estimates the spherically symmetric model for a wormhole.[58]

The scattering of signals on spherical wormholes has been previously studied in Refs. 55, 56, and 58 Consider first the case of a static gas of wormholes, i.e. in the absence of peculiar motions. The spherical wormhole can be considered as a couple of conjugated spherical mirrors. When a relict photon falls on one mirror, a reflected photon is emitted, upon the scattering, from the second (conjugated) mirror. The cross-section of such a process has been derived in Ref. 58 and can be summarized as follows. Let an incident plane wave (a set of photons) falls on one throat. Then, the scattered signal has two parts. First part represents the standard diffraction (which corresponds to the absorption of CMB photons on the throat) and forms a very narrow beam along the direction of the propagation. This is the so-called scattering forward which is described by the cross-section

$$\frac{d\sigma_{\rm absor}}{d\Omega} = \sigma_0 \frac{(ka)^2}{4\pi} \left| \frac{2J_1(ka\sin\chi)}{ka\sin\chi} \right|^2,$$

where $\sigma_0 = \pi a^2$, a is the radius of the throat, k is the wave vector, and χ is the angle from the direction of propagation of the incident photons, and J_1 is the Bessel function. Together with this part the second throat emits an omnidirectional isotropic flux with the cross-section

$$\frac{d\sigma_{\rm emit}}{d\Omega} = \sigma_0 \frac{1}{4\pi}. \tag{12}$$

It is easy to check that the total cross-sections coincide

$$\int \frac{d\sigma_{\rm absor}}{d\Omega} d\Omega = \int \frac{d\sigma_{\rm emit}}{d\Omega} d\Omega = \sigma_0,$$

which is equivalent to a conservation law for the number of photons (the number of absorbed and emitted photons coincides). This is enough to understand what is going on with CMB in the presence of the gas of wormholes. In the absence of peculiar motions, every end of a wormhole throat absorbs photons as the absolutely black body, while the second throat end re-radiates them in an isotropic manner (with the black body spectrum). It is clear that there will not appear any distortion of the CMB spectrum at all. In other words, we may say that in the absence of peculiar motions the distortion of the spectrum does not occur.

Consider now the presence of peculiar motions. The motion of one wormhole throat end with respect to CMB causes the angle dependence of the incident radiation with the temperature

$$\begin{aligned} T_1 &= \frac{T_\gamma}{\sqrt{1-\beta_1^2}(1+\beta_1\cos\theta_1)} \\ &\simeq T_\gamma(1-\beta_1\cos\theta_1+\cdots), \end{aligned}$$

where $\beta_1 = V_1/c$ is the velocity of the throat end and $\beta_1\cos\theta_1 = (\boldsymbol{\beta}_1\mathbf{n}), \mathbf{n}$ is the direction for incident photons. Therefore, the absorbed radiation has the spectrum

$$\rho(T_1) = \rho(T_\gamma) + \frac{d\rho(T_\gamma)}{dT}\Delta T_1 + \frac{1}{2}\frac{d^2\rho(T_\gamma)}{dT^2}\Delta T_1^2 + \cdots,$$

where $\rho(T_\gamma)$ is the standard Planckian spectrum and $\Delta T_1(\beta_1\cos\theta_1) = T_1 - T_\gamma$. It turns out that to the first-order in β_1 such an anisotropy gives no contribution in the re-radiated photons and does not contribute in the distortion of the spectrum. Indeed, in the reference system in which the second end of the throat is at rest we have the isotropic flux (12) and, therefore, integrating over the incident angle θ_1, we find $\int \Delta T(\cos\theta_1)d\Omega = 0$. This means that to the first-order in β_1 the second end of the throat radiates (in the rest reference system) the same blackbody radiation with the same temperature T_γ. To next orders in β_1, a nonvanishing contribution to the distortion of the spectrum $\rho(T_1) - \rho(T_\gamma)$ appears. However, to next orders, a

more important feature will appear, when we consider the actual wormhole sections in the form of tori. We consider such details elsewhere.

Consider now the re-radiation of the absorbed CMB photons. In the first-order by $\beta_2 = V_2/c$ (V_2 is the peculiar velocity of the second end of the wormhole throat) it radiates the black body radiation with the apparent surface temperature (brightness)

$$T_2 \simeq T_\gamma(1 + \beta_2 \cos\theta_2 + \cdots), \tag{13}$$

where $\beta_2 \cos\theta_2 = (\boldsymbol{\beta}_2 \mathbf{m})$ and $\mathbf{m}$ is the unit vector pointing out to the observer. This is exactly the kinematic SZ effect.

Consider a collection (cloud) of wormhole throats. Chaotic peculiar motions of different wormholes do not contribute to the CMB distortion (at least if wormholes are not too big). We may expect to observe only coherent motions of the cloud. To obtain the net energy–momentum transfer between the CMB radiation and the gas of wormholes, we have to average over the wormhole, distribution. On average CMB photons undergo τ_w scatterings, where τ_w is the projected cloud optical depth due to the scattering. If $n(r)$ is the number density of wormholes measured from the center of the cloud, then τ_w is given by $\tau_w = \pi\overline{a^2}\int n(r)d\ell$, where the integration is taken along the line of sight and $\overline{a^2} = \frac{1}{n}\int a^2 n(r,a)da$. Here $n(r,a)$ is the number density of wormholes depending on the throat radius a. Since all wormhole throats have the surface brightness (see Eq. (13)) which is different from that of CMB, the parameter τ_w defines (together with the peculiar velocity of the cloud β_2) the surface brightness of the cloud itself.

5.2. *Polarization of the SZ effect*

Despite the unique possible applications of the kinematic SZ effect as galaxy cluster speedometer, it is worth stressing once more that the use of the kinematic SZ effect to retrieve galaxy clusters motions only provides an indication on the electrons peculiar velocity along the line of sight. On the other hand, transverse motions may in principle be studied through the SZ effect when its polarization will be detected.

The SZ effect is expected to be polarized at levels proportional to powers of (v_p/c) and τ. Polarization in the SZ effect mainly arises from four different processes, all invoking the presence of a quadrupole:

- the first one is due to the radiation quadrupole due to the thermal SZ effect itself, which is generated by a previous scattering elsewhere in the cores of the local and nearby clusters. This is thus a double scattering process;
- the second one is similar to the first one but it is due to the kinematic effect;
- the third one is due to the radiation quadrupole due to Doppler shift caused by the intrinsic peculiar velocity of the electron gas in the plane normal to the line of sight;

- the fourth one is due to the scattering of the CMB intrinsic quadrupole and free electrons in the cluster of galaxy.

The first polarization effect originates from the anisotropic optical depth to a given location in the cluster. For example, toward the outskirts of a cluster one expects to see concentric (radial) patterns of the linear polarization at frequencies where the thermal SZ effect is positive (negative). It is thus due to the anisotropy in the radiation field in the direction of the cluster center due to the thermal SZ effect itself. Nevertheless, nonspherical morphology for the electron distributions will lead to considerably complicated polarization patterns. The peak polarization of this signal will be order of τ times the SZ effect signal, i.e. $\sim 0.01\Theta_e\tau^2$. In principle, this effect could be used to measure the optical depth of the cluster and therefore to separate T_e and τ from a measurement of the thermal SZ effect.

In the case of double scattering originating from kinematic SZ effect (second case), the effect is also sensitive to the transverse ICM peculiar velocity and the intensity is expected to be $\sim 0.01\tau^2(v_p/c)$. Using $\tau = 0.01$ and a bulk motion of $500\,\mathrm{km\,s^{-1}}$, results in maximum polarization levels of order few nK, beyond the sensitivity of current instrumentation.

The third case is unambiguously sensitive to the ICM velocity in the direction transverse to the line of sight. In fact, in the case of polarization directly due to the motion of the cluster with respect to the CMB, and transverse to our line of sight, the quadrupole comes from the Doppler shift. This effect has been found to be $\sim 0.1\tau(v_p/c)^2$, again at the nK level even for hot clusters.[66,108,116]

The fourth polarization possibility is due to Thomson scattering of the intrinsic CMB quadrupole by the free electron of the ICM. Sazonov and Sunyaev[108] calculated the expected polarization level and found the maximum CMB quadrupole induced polarization is few $\tau \times 10^{-6}$K, somewhat higher than the expected velocity induced terms discussed above. Even if it is still too small to expect detection in the near future, this mechanism could possibly be used to trace the evolution of the CMB quadrupole if polarization measurements could be obtained for a large number of clusters binned in direction and redshift.

Despite in all cases the expected level of SZ polarization is lower than the current instrumental sensitivity and the current ability to disentangle cosmological effects from foregrounds, once the different SZ polarization will be able to be disentangled, the SZ polarization will represent a unique possibility to make 3D studies of galaxy cluster motions.

6. Spectrometric Measurements of the SZ Effect

Most of the effects described in this review can only be studied with multifrequency detections of the SZ effect. All of them would greatly benefit from spectroscopic measurements of the SZ with moderate spectral resolution (i.e. 5–10 GHz). In addition, the capability to disentangle the SZ effect from foregrounds, such as thermal

dust emission, free–free and synchrotron, is directly dependent by the number of spectral channels one makes the observations with. Cosmological effects such as the deviation of the absolute CMB temperature from a standard adiabatic scenario, detectable with the *M-R* method, show their biggest effects in the "cross-over" band (i.e. $\sim 217\,\mathrm{GHz}$). Astrophysical effects as the presence of nonthermal component caused by e.g. AGNs, relativistic plasma, shock acceleration or dark matter (neutralinos) are predicted to be important in the sub-mm region.[22] The possibility to disentangle thermal SZ, kinematic SZ and its relativistic corrections, and to determine the physical parameters of the galaxy clusters such as optical depth, plasma temperature, peculiar velocity etc. requires detailed spectral informations in the whole mm range. de Bernardis *et al.*[26] have shown that a differential spectrometer covering four bands with a resolution of $\sim 6\,\mathrm{GHz}$ eliminates most of the bias resolution in a full recovery of the input cluster parameters. This possibility is clearly hampered in ground-based few-band photometers while spectrometers suitable for balloon borne observations or for dedicated space missions would make the necessary step forward.

An early effort was produced by the Italian astrophysical community for the construction of the Spectroscopic active galaxies and cluster explorer (SAGACE) experiment proposed to the Italian space agency for a small mission Earth-orbit satellite with the intent to use a 3 m diameter primary mirror coupled to a Fourier transform spectrometer (FTS).[27] More recently, the OLIMPO experiment[72] has been upgraded with a differential FTS[23,109] taking advantage of the clean conditions that a balloon borne experiment can find in the stratosphere. OLIMPO will be launched on June 2017 from Svalbard Islands and will represent the first possibility to explore the use of a FTS coupled with a four-band photometer in the millimetric and sub-millimetric range. Simulations[26] show that even a warm spectrometer, mounted on a balloon borne experiment like OLIMPO,[72] allows an unbiased recovery of the galaxy cluster thermal optical depth, electron temperature, dust contamination, non-thermal optical depth, despite being still limited at high frequencies by radiative background. A low earth-orbit satellite like SAGACE[27] improves the capability to detect non-thermal effects and the disentangling from foregrounds. A Sun-Earth Lagrangian point L2 spectrometer like the one proposed for the Spectrum-M — millimetron mission[28] allows an exquisite recovery of the input parameters with better than 10% precision with no need to include strong priors on the input parameters.

This experimental activity is clearly connected to the renewed interest, in the scientific cosmological community, to the possibility to detect the deviation from a black body in the frequency spectrum of the CMB[21] and the experimental effort going on especially for the preparation of the next CMB space mission for this goal.[3,62]

Acknowledgments

The authors who are members of the *Planck* Collaboration warmly thank the *Planck* Collaboration for numberless and constructive conversations on the subjects discussed here. Some of the results in this paper have been derived using the HEALPix[42] package. We acknowledge the use of the NASA Legacy Archive for microwave Background Data Analysis (LAMBDA) and of the ESA *Planck* Legacy Archive. C. Burigana and M. Rossetti acknowledge partial support by ASI/INAF Agreement 2014-024-R.1 for the *Planck* LFI Activity of Phase E2. Some of the results presented here are based on CFHT observations processed at the TERAPIX data center located at IAP/France. We thank Gemma Luzzi for Fig. 2 on the $T_{\rm CMB}$ versus z scaling relation. We acknowledge the use of the SZ-Cluster Database operated by the Integrated Data and Operation Center (IDOC) at the Institut d'Astrophysique Spatiale (IAS) under contract with CNES and CNRS.

References

1. R. Adam *et al.*, *Astron. Astrophys.* **576** (2015) A12.
2. AMI consortium, *Mon. Not. R. Astron. Soc.* **433** (2013) 2036.
3. P. Andre *et al.*, *J. Cosmol. Astropart Phys.* **02** (2014) 006.
4. A. Avgoustidis *et al.*, arXiv:astro-ph/1511.04335.
5. S. Basilakos, *Mon. Not. R. Astron. Soc.* **344** (2003) 602.
6. M. Batiste and D. J. Batuski, *Mon. Not. R. Astron. Soc.* **436** (2013) 3331.
7. E. S. Battistelli *et al.*, *Astrophys. J.* **580** (2002) 101.
8. E. S. Battistelli *et al.*, *Astrophys. J.* **598** (2003) L75.
9. E. S. Battistelli *et al.*, *Astrophys. J.* **645** (2006) 826.
10. B. A. Benson *et al.*, *Astrophys. J.* **592** (2003) 674.
11. M. Birkinshaw, *Phys. Rep.* **310** (1999) 97.
12. L. E. Bleem *et al.*, *Astrophys. J. Suppl.* **216** (2015) 27.
13. M. Bonamente *et al.*, arXiv:astro-ph/1112.1599.
14. M. Bonamente *et al.*, *New J. Phys.* **14** (2012) 025010.
15. D. A. Buote *et al.*, *Astrophys. J.* **695** (2009) 1351.
16. M. Calvo *et al.*, arXiv:astro-ph/1601.02774.
17. J. R. Carlstrom *et al.*, *Ann. Rev. Astron.* **40** (2002) 643.
18. R. Cen and K. P. Ostriker, *Astrophys. J.* **519** (1999) L109.
19. A. Challinor and A. Lasemby, *Astrophys. J.* **499** (1998) 1.
20. J. Chluba, *Mon. Not. R. Astron. Soc.* **442** (2014) 1881.
21. J. Chluba, arXiv:astro-ph/1405.6938.
22. S. Colafrancesco *et al.*, *Astron. Astrophys.* **397** (2003) 27.
23. G. D'Alessandro *et al.*, *Ap. Opt.* **54** (2015) 9269.
24. N. D'Amico, *AIPC* **1357** (2011) 317.
25. R. Davé, R. Cen and K. P. Ostriker, *Astrophys. J.* **552** (2001) 473.
26. P. de Bernardis *et al.*, *Astron. Astrophys.* **538** (2012) A86.
27. P. de Bernardis *et al.*, arXiv:astro-ph/1002.0867.
28. P. de Bernardis *et al.*, *Am. Astron. Soc.* **223** (2014) 340.04.
29. de Martino. *et al.*, *Astrophys. J.* **808** (2015) 128.
30. M. De Petris *et al.*, *Astrophys. J.* **574** (2002) L119.

31. S. R. Dicker *et al.*, *Proc. SPIE* **7020** (2008) 702005.
32. S. R. Dicker *et al.*, *Proc. SPIE* **9153** (2014) 91530J.
33. R. Dünner *et al.*, *Mon. Not. R. Astron. Soc.* **366** (2006) 803.
34. D. Eckert *et al.*, *Astron. Astrophys.* **551** (2013) A22.
35. R. Fabbri, F. Melchiorri and V. Natale, *Astrophys. Space. Sci.* **59** (1978) 2237.
36. R. Fabbri, *Astrophys. Space. Sci.* **77** (1981) 529.
37. C. Ferrari, *Astron. Astrophys.* **534** (2011) 12.
38. L. Feretti, *Astron. Astrophys. Rev.* **20** (2012) 54.
39. M. Fukugitai, *Astrophys. J.* **503** (1998) 518.
40. R. Genova-Santos *et al.*, *Mon. Not. R. Astron. Soc.* **363** (2005) 79.
41. J. Glen *et al.*, *Proc SPIE* **3357** (1998) 326.
42. K. M. Gorski *et al.*, *Astrophys. J.* **622** (2005) 759.
43. T. Goto *et al.*, *Astron. J.* **123** (2002) 1807.
44. N. Hand *et al.*, *Phys. Rev. Lett.* **109** (2012) 041101.
45. M. Hasselfield *et al.*, *J. Cosmol. Astropart Phys.* **7** (2013) 8.
46. A. Hincks *et al.*, *Astrophys. J. Suppl.* **191** (2010) 423.
47. H. Hoekstra *et al.*, *Mon. Not. R. Astron. Soc.* **449** (2015) 685.
48. W. L. Holzapfel *et al.*, *Astrophys. J.* **480** (1997) 449.
49. C. Horellou *et al.*, *Astron. Astrophys.* **441** (2005) 435.
50. N. Itoh *et al.*, *Astrophys. J.* **502** (1998) 7.
51. N. Itoh *et al.*, *Mon. Not. R. Astron. Soc.* **327** (2001) 567.
52. A. Kashlinsky *et al.*, arXiv:astro-ph/1012.3214.
53. A. A. Kirillov and D. Turaev, *Mon. Not. R. Astron. Soc.* **371** (2006) L31.
54. A. A. Kirillov and E. P. Savelova, *Phys. Lett. B* **660** (2008) 93.
55. A. A. Kirillov *et al.*, *Phys. Lett. B* **663** (2008) 372.
56. A. A. Kirillov *et al.*, *JETP Lett.* **90** (2009) 599.
57. A. A. Kirillov and E. P. Savelova, *Mon. Not. R. Astron. Soc.* **412** (2011) 1710.
58. A. A. Kirillov and E. P. Savelova, *Phys. Lett. B* **710** (2012) 516.
59. A. A. Kirillov and E. P. Savelova, arXiv:astro-ph/1505.05101.
60. A. A. Kirillov, *Proceedings of the Fourteenth Marcel Grossman Meeting on General Relativity*, eds. M. Bianchi, R. T. Jantzen and R. Ruffini, in press.
61. T. Kitayama, *Prog. Theor. Exp. Phys* **06B111** (2014).
62. A. Kogut *et al.*, *Proc. SPIE* **9143** (2014) 91431E17.
63. E. Komatsu *et al.*, *Publ. Astron. Soc. Jpn.* **53** (2001) 57.
64. A. S. Kompaneets, *Soviet Phys. JETP* **4** (1957) 730.
65. L. Lamagna *et al.*, *New Astronomy* **51** (2007) 381.
66. G. Lavaux *et al.*, *Mon. Not. R. Astron. Soc.* **347** (2004) 729.
67. J. A. S. Lima *et al.*, *Mon. Not. R. Astron. Soc.* **312** (2000) 747.
68. J. M. LoSecco *et al.*, *Phys. Rev. D* **64** (2001) 123002.
69. G. Luzzi *et al.*, *Astrophys. J.* **705** (2009) 1122L.
70. G. Luzzi *et al.*, *J. Cosmol. Astropart Phys.* **09** (2015) 011L.
71. B. S. Mason *et al.*, *Astrophys. J.* **716** (2010) 739.
72. S. Masi *et al.*, *Mem.S.A.It* **79** (2008) 887.
73. P. Mazzotta *et al.*, *Astrophys. J.* **675** (2008) L9.
74. F. Melchiorri *et al.*, Background microwave radiation and intracluster cosmology, in *Proceedings of the International School of Physics "Enrico Fermi", Course CLIX*, held at Verenna on Lake Como, Villa Monastero, July 6–16, 2005, eds. F. Melchiorri and Y. Rephaeli (IOS Press, The Netherlands, Italy, 2005), p. 225.

75. J.-B. Melin and J. G. Bartlett, *Astron. Astrophys.* **578** (2015) A21.
76. F. Menanteau *et al.*, *Astrophys. J.* **748** (2012) 7.
77. P. Merluzzi *et al.*, *Mon. Not. R. Astron. Soc.* **446** (2014) 803.
78. S. Muller *et al.*, *Astron. Astrophys.* **551** (2013) 109.
79. K. Nandra *et al.*, arXiv:astro-ph/1306.2307.
80. F. Nicarstro *et al.*, *Astrophys. J.* **629** (2005) 700.
81. S. Nozawa *et al.*, *Astrophys. J.* **508** (1998) 17.
82. A. L. O'Mill *et al.*, *Mon. Not. R. Astron. Soc.* **453** (2015) 868.
83. A. L. O'Mill *et al.*, *Proceedings of the Fourteenth Marcel Grossman Meeting on General Relativity*, eds. M. Bianchi, R. T. Jantzen and R. Ruffini, in press.
84. P. Ostermann, *Proceedings of the Twelfth Marcel Grossman Meeting on General Relativity*, eds. T. Damour, R. T. Jantzen and R. Ruffini (World Scientific, Singapore, 2012), p. 1408. ISBN 978-981-4374-51-4.
85. P. Ostermann, *Proceedings of the Twelfth Marcel Grossman Meeting on General Relativity*, eds. T. Damour, R. T. Jantzen and R. Ruffini (World Scientific, Singapore, 2012), p. 1373. ISBN 978-981-4374-51-4.
86. P. Ostermann, digIT Verlag (2014).
87. T. J. Plagge *et al.*, *Astrophys. J.* **770** (2013) 112.
88. Planck Collab., *Astron. Astrophys.* **536** (2011) A8.
89. Planck Collab., *Astron. Astrophys.* **550** (2013) A131.
90. Planck Collab., *Astron. Astrophys.* **554** (2013) A140.
91. Planck Collab., *Astron. Astrophys.* **550** (2013) A134.
92. Planck Collab., *Astron. Astrophys.* **571** (2014) A20.
93. Planck Collab., *Astron. Astrophys.* **571** (2014) A29.
94. Planck Collab., *Astron. Astrophys.* **580** (2015) A22.
95. Planck Collab., arXiv:astro-ph/1502.01597.
96. Planck Collab., arXiv:astro-ph/1502.01598.
97. Planck Collab., arXiv:astro-ph/1502.01589.
98. Planck Collab., arXiv:astro-ph/1502.01596.
99. E. D. Reese *et al.*, *Astrophys. J.* **721** (2010) 653.
100. Y. Rephaeli, *Astrophys. J.* **241** (1980) 858.
101. Y. Rephaeli, *Ann. Rev. Astron. Astrophys.* **33** (1995) 541.
102. Y. Rephaeli, *Astrophys. J.* **445** (1995) 33.
103. Y. Rephaeli *et al.*, *Nuouo Cimento* **291** (2006) 1.
104. C. E. Romero *et al.*, *Astrophys. J.* **807** (2015) 121.
105. J. Sayers *et al.*, *Astrophys. J.* **778** (2013) 52.
106. A. Saro *et al.*, *Mon. Not. R. Astron. Soc.* **440** (2014) 2610.
107. J. Sayers *et al.*, *Astrophys. J.* **768** (2013) 177.
108. S. Y. Sazonov and R. A. Sunyaev, *Mon. Not. R. Astron. Soc.* **310** (1999) 765.
109. A. Schillaci *et al.*, *Astron. Astrophys.* **565** (2014) A125.
110. M. Shimon and Y. Rephaeli, *New Astron.* **9** (2004) 69.
111. J. M. Shull *et al.*, *Astrophys. J.* **759** (2012) 23.
112. Z. Stanieszewski *et al.*, *Astrophys. J.* **701** (2009) 32.
113. I. F. Suarez-Velaquez, *et al.*, *Astrophys. J.* **431** (2013) 342.
114. R. A. Sunyaev and Y. B. Zeldovich, *Com. Astroph. Sp. Ph.* **2** (1970) 66.
115. R. A. Sunyaev and Y. B. Zeldovich, *Com. Astroph. Sp. Ph.* **4** (1972) 173.
116. R. A. Sunyaev and Y. B. Zeldovich, *Mon. Not. R. Astron. Soc.* **190** (1980) 413.
117. R. A. Sunyaev and Y. B. Zeldovich, *Ann. Rev. A* **18** (1980) 537.

118. J. Tinker and A. V. Kravtsov *et al.*, *Astrophys. J.* **688** (2008) 709.
119. T. M. Tripp, *et al.*, *Astrophys. J. Suppl.* **177** (2008) 39.
120. L. Van Waerbeke *et al.*, *Phys. Rev. D* **89** (2014) 023508.
121. A. Von der Linden *et al.*, *Mon. Not. R. Astron. Soc.* **443** (2014) 1973.
122. E. L. Wright, *Astrophys. J.* **232** (1970) 348.
123. Y. Yao *et al.*, *Astrophys. J.* **746** (2012) 166.
124. C. Zhang *et al.*, arXiv:astro-ph/1406.4019.